NANO · MICRO small
www.small-journal.com

Solar Energy Storage Using a Cu_2O-TiO_2 Photocathode in a Lithium Battery

*Isabel Ciria-Ramos, Emilio J. Juarez-Perez, and Marta Haro**

A Cu_2O-TiO_2 photoelectrode is pr+oposed for simultaneous solar light energy harvesting and storing of electrochemical energy in an adapted lithium coin cell. The p-type Cu_2O semiconductor layer is the light harvester component of the photoelectrode and the TiO_2 film performs as the capacitive layer. The rationale of the energy scheme shows that the photocharges generated in the Cu_2O semiconductor induce lithiation/delithiation processes in the TiO_2 film as a function of the applied bias voltage and light power. A photorechargeable lithium button cell drilled on one side recharges with visible white light in ≈9 h in open circuit. It provides an energy density of ≈150 mAh g^{-1} at 0.1 C discharge current in dark, and the overall efficiency is 0.29%. This work draws a new approach for the photoelectrode role to advance in monolithic rechargeable batteries.

1. Introduction

The transition from fossil-based energy to renewable energy sources is a burgeoning need for decarbonization and for a sustainable energy and economic model. Renewable energy sources, such as solar energy, have a huge potential, but their utilization is limited due to their fluctuating and intermittent nature. Thus, solar cells often work with batteries in complement to satisfy the imbalances in production and consumption. In contrast to the use of two physically separate devices for production (photovoltaic device) and storage (battery), a monolithic assembly of these two devices sharing a common electrode can be interesting in certain applications where device shape factor, portability and decentralization of energy production and storage are more important properties than overall process effectiveness. The solar electrochemical energy storage (SEES) concept was first proposed by Hodes in 1976,[1] based on a photoelectrochemical cell, using CdSe as a photoelectrode, S/S^{-2} as the redox electrolyte and Ag_2S/Ag as an anode. Pioneering research in solar electrochemical energy storage systems was eclipsed by the coetaneous reported solar water splitting[2] and advanced oxidative processes[3] with more promising results and higher effective use of the solar energy. However, the interest in these studies has increased in the last decade due to socio–political requirements for decentralized and sustainable energy and technological advances in electrochemical energy power sources (particularly in Li-ion batteries), and photovoltaic cells (such as dye-sensitized and perovskite solar cells). Even though this renewed interest, studies of SEES systems based on intercalation ion batteries are still scarce. In the early 2000s, the SEES systems were based on dye-sensitized solar cells. In these systems, the electrolyte contains the redox pair I_3^-/I^-, which interchanges the charges with a Pt cathode while the anode can intercalate/chemisorb ions (Li^+ or ClO_4^-) promoted by the charges generated in the photoelectrode TiO_2 sensitized with dye particles.[4–9] Based on the same approach, SEES systems were extended to Li-ion batteries promoting the delithiation of the cathodes, such as Li—O_2,[10–12] Li—S,[13] and $LiFePO_4$,[14,15] or other cations, such as Na^+.[16] In the last few years, the approach to achieve SEES systems was modified from the adaptation of dye-sensitized solar cell to the design of the battery itself using a semiconductor electrode with the dual functionality of light harvesting and electrochemical energy storage based on lithium[17–20] or zinc ion.[21–24] This approach signifies an important advance since photocapacitive device is fabricated as current working batteries with conversion efficiency energies ranging from 0.03% to 1.2%.[18,21,23] However, in these systems the light harvesting material is the "acceptor" of the photoholes that induce the deintercalation process while the electrons travel to the counter electrode. A single material for both capacitive and light harvesting functions affects the system operation and hampers a succinct interpretation of the physical processes since the ion intercalation induces changes in the electrical properties of the semiconductor.

I. Ciria-Ramos, E. J. Juarez-Perez, M. Haro
Instituto de Nanociencia y Materiales de Aragón (INMA)
CSIC-Universidad de Zaragoza
Zaragoza 50009, Spain
E-mail: mharo@unizar.es

I. Ciria-Ramos, M. Haro
Departamento de Química Física
Facultad de Ciencias
Universidad de Zaragoza
Plaza San Francisco
Zaragoza 50009, Spain

E. J. Juarez-Perez
Aragonese Foundation for Research and Development (ARAID)
Government of Aragon
Zaragoza 50018, Spain

The ORCID identification number(s) for the author(s) of this article can be found under https://doi.org/10.1002/smll.202301244.

DOI: 10.1002/smll.202301244

In a previous study, a photocapacitive system was developed based on $BiVO_4$ light harvester and PbO_x nanoparticles performing the capacitive platform by redox pesudocapacitance.[25,26] Based on this idea, the proposed photoelectrode in this work consists of separating the photovoltaic and the energy storage elements in two different layers: a TiO_2 capacitive film deposited on p-type Cu_2O light harvester film. The optical and electrochemical characterization of Cu_2O and TiO_2 films were analyzed separately by UV–vis and UPS spectroscopy and in a lithium semibattery cell, respectively. This analysis allows to have an energetic landscape of the studied system that explains the linear sweep voltammetry with chopped light and the cyclic voltammetry at different light powers. Then, our Cu_2O-TiO_2/Li photobattery based on photocathode and metal anode is able to photocharge under one Sun of white LED light in open circuit providing ≈150 mAh g^{-1} of energy density when discharged at 0.1C in dark. The overall efficiency of the output electric energy with respect to the light energy emitted by the LED is 0.29%. This value is approximately an order of magnitude above the reported values for the photocharge of lithium-based batteries,[14,18] and similar to zinc-based batteries.[23] Beyond the photorechargeable lithium battery, this study provides insight into the energy band requirements of materials to design photoelectrodes suitable for next-generation photorechargeable batteries in which the metal electrode would be replaced by another type of anode/cathode electrode.

2. Results and Discussion

2.1. Synthesis and Characterization of p-Semiconductor Cu_2O: Light Harvester

SEM images of electrodeposited Cu_2O show prismatic crystals of 2–4 µm with smooth [111] facets,[27] inset **Figure 1**a. XRD diffractogram (Figure 1a) identifies the face-centered cubic Cu_2O phase without detectable presence of CuO or Cu traces.[28] XPS spectrum (Figure S7, Supporting Information) confirms +1 as state of oxidation of copper. XPS also detects the presence of CuO due to minor surface oxidation of Cu_2O.[29]

The optical absorption $F(R_\infty)$ of Cu_2O film (Figure S2a, Supporting Information) shows broad absorbance in the visible region with an edge at about 600 nm, in agreement with the red-brown color of Cu_2O (Figure S2d, Supporting Information). The extrapolated value estimates a Tauc gap of 1.97 eV ± 0.02 eV (Figure 1b), value in good agreement with the literature.[28,30]

UPS spectrum (Figure 1c) shows the position of the valence-band maximum with reference to the Fermi level of the instrument (VBMF), determined by the extrapolation of the steepest descent of the leading edge of the spectrum to the base line .[31] The estimated VBMF is 0.76 eV. This value is almost the half energy of the Cu_2O film bandgap, thus the p-character of the film is weak at difference than other similar electrodeposited films.[32] The secondary electron cut off (SECO) zone shows a vertical drop over 16.94 eV. Then, the absolute VB with reference to vacuum level is VB = SECO − $h\nu$ − VBMF = −5.02 eV. The CB is estimated by adding the E_g calculated by the Tauc plot: CB = −5.02 + 1.97 = −3.05 eV. These estimated values are in the order of the reported values in the literature,[29,33,34] within the disparity of the values due to the influence of the synthesis method on the electric properties and the experimental uncertainty of the measurement.

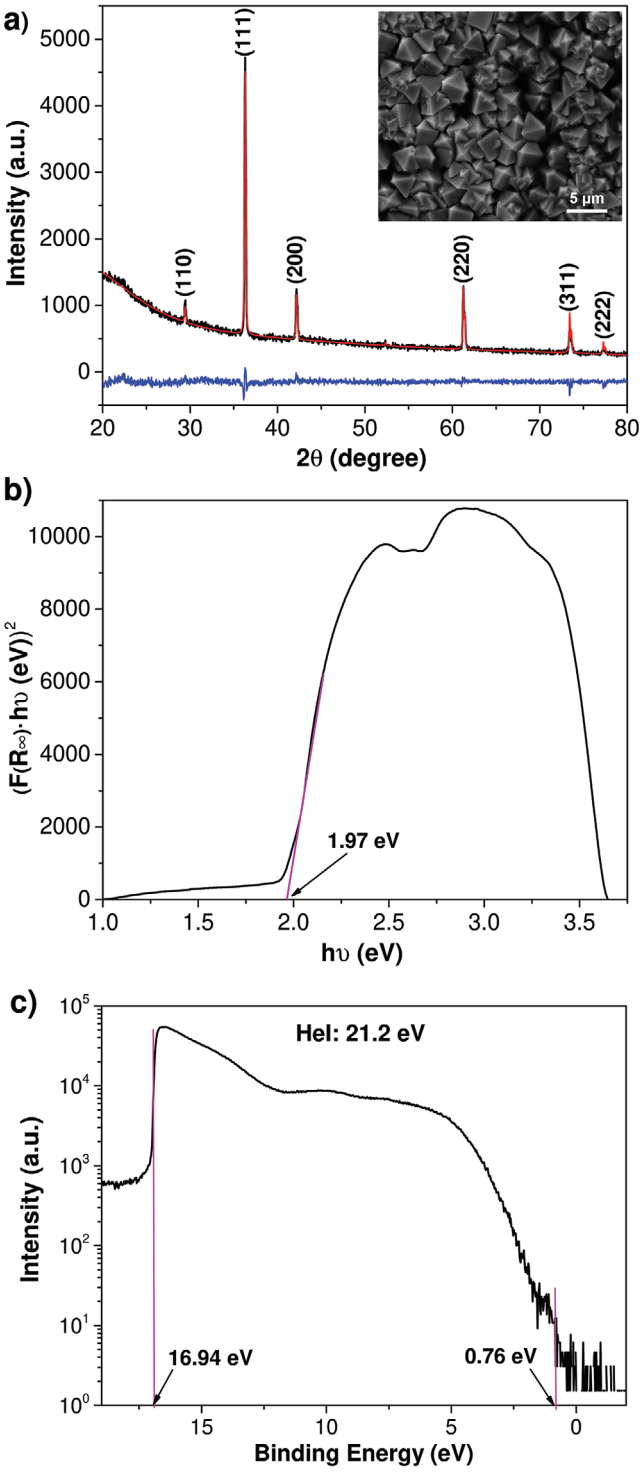

Figure 1. Characterization of electrodeposited Cu_2O film. a) XRD spectrum of the Cu_2O film (black), the fitting to a cuprite phase (red), and the intensity difference of the fitting (blue). Inset: SEM image of the film obtained at a magnification of 10 000. b) Cu_2O bandgap estimation from the Tauc plot profile. c) UPS of Cu_2O film measured with the 21.2 eV excitation energy corresponding to HeI radiation.

2.2. Synthesis and Characterization of TiO_2 Anode: Capacitive Element

XRD diffractogram (**Figure 2**a) confirms the formation of pure anatase without detectable presence of rutile or brookite phase. The average size of TiO_2 nanoparticles was 11.2 ± 0.2 nm obtained from X-ray diffraction data and qualitatively confirmed by SEM microscopy (inset Figure 2a). The Tauc plot obtained from the UV–vis spectra estimates a bandgap of 3.24 eV confirming that TiO_2 nanoparticles only absorb in the UV region of the spectrum, Figure 2b.

The capacitive response of the synthesized TiO_2 nanoparticles was tested as electrode in Li semibattery configuration. The cyclic voltammetry (CV) (Figure 2c) shows cathodic and anodic peaks at 1.7 V (−3.2 eV) and 2.0 V (−3.5 eV) versus Li/Li^+ (vs energy vacuum scale), respectively.[35] The mid value 1.85 V (−3.35 eV) corresponds to the work function of Li_xTiO_2/TiO_2 redox pair that appears above the CB of TiO_2 at −3.95 eV.[36] The energy difference between the work function and the CB is because the lithium adsorption/intercalation transport can only develop at determined TiO_2 positions or channels, besides the effect of electron and cation concentration at the electrode/electrolyte interface.[37,38] The CV has quasi-rectangular shape between 1 and 2.3 V versus Li/Li^+ indicating a relevant contribution of pseudocapacitance. This pseudocapacitance originates from the nanoparticle size of TiO_2 that boost surface reactions [39] allowing a fast charge–discharge of the electrode of 100 mAh g^{-1} at 10 C (Figure S8, Supporting Information).

2.3. Working Mechanism of the Cu_2O-TiO_2 Photoelectrode

The complete photoelectrode consists of a TiO_2 film (≈ 1 mg cm^{-2}) deposited on the electrodeposited Cu_2O on ITO substrate. The photoelectrochemical study was performed using white light LED without UV irradiation exciting the TiO_2 layer (Figure S5, Supporting Information). The electrochemical voltage window is between 2.6 and 1.6 V versus Li/Li^+ avoiding the solid electrolyte interface (SEI) formation [40] or lithiation processes in the Cu_2O film (Figure S9, Supporting Information). The Cu_2O-TiO_2 photoelectrode was placed in the modified CR2032 coin cell (Figure S4a, Supporting Information) allowing the illumination of the Cu_2O side while TiO_2 layer faces the electrolyte and lithium counter electrode.

Figure 3a depicts the basic elements of the photoelectrode energetic landscape showing the conduction band (CB) and valence band (VB) energy levels of Cu_2O and TiO_2 films. The cathodic peak of the CV settles above the work function of the TiO_2/Li_xTiO_2 system dash line pointing to the electrode lithiation: $TiO_2 + xLi^+ + xe^- \rightarrow Li_xTiO_2$. The reverse reaction (delithiation) occurs as the anodic peak below this work function energy level.

The CVs of the photoelectrode registered at different light power and dark are represented in Figure 3b. Cu_2O semiconductor absorbs photons promoting electrons from the VB into the CB proportionally to the light power. At 25 mW cm^{-2}, the cathodic peak matches with the obtained at dark. At 50 mW cm^{-2}, a second cathodic peak appears at 1.73 V versus Li/Li^+. At ≥75 mW cm^{-2}, only one cathodic peak appears at 1.73 V versus Li/Li^+ with increased intensity as the light power rises. Contrarily, the anodic peak voltages displace and the intensity increases continuously with the light power. The CB of Cu_2O (Figure 3a) matches with the energy empty states of Li_xTiO_2 and the photoinduced reduction process is

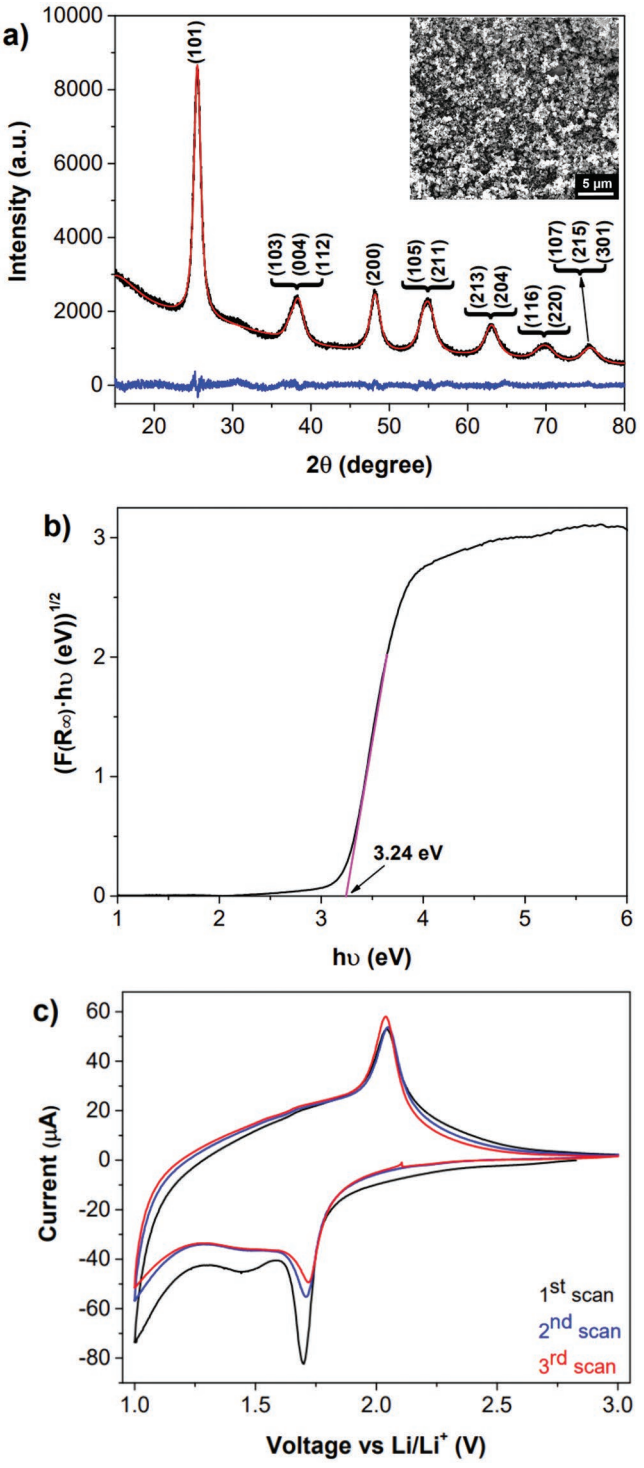

Figure 2. Characterization of TiO_2 particles and film. a) XRD spectrum of TiO_2 particles (black), the fitting to anatase phase (red), and the intensity difference of the fitting (blue). Inset: SEM image of the film obtained at a magnification of 10 000. b) Tauc plot of the Kubelka–Munk transformation of the total reflectance data. c) First three cycles of a TiO_2/Li semibattery CV measured at a scan rate of 0.1 mV s^{-1}.

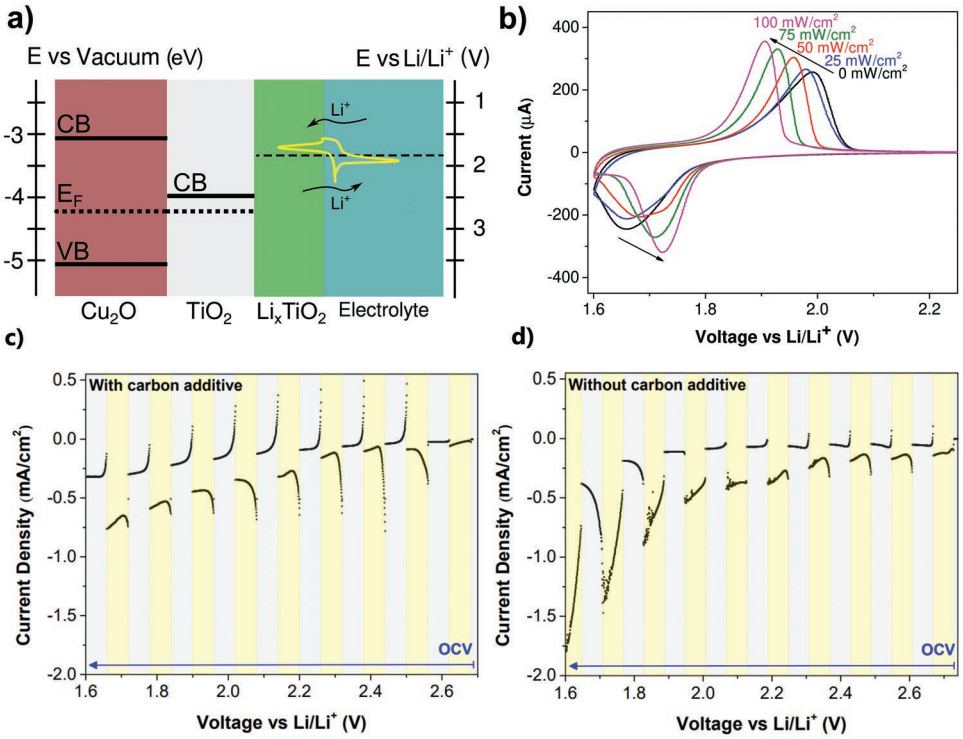

Figure 3. Cu_2O-TiO_2 photoelectrode characterization. a) Energetic landscape of the photoelectrode containing Cu_2O-TiO_2 and surface Li_xTiO_2 in contact with the electrolyte. At TiO_2/electrolyte interface, the CV of lithiation/delithiation processes is depicted, corresponding to the empty and fill states of Li_xTiO_2 and the work function as the dash line. The energetic scales are respect vacuum (left) and Li/Li^+ reference electrode (right). b) CV plots of Cu_2O-TiO_2 photoelectrode in the semibattery in dark and under several light illumination powers. LSV plot under chopped light of 5 min intervals in cathodic direction at 0.2 mV s^{-1} of Cu_2O-TiO_2 photoelectrode: c) TiO_2 film contains carbon black additive (10% w) and d) TiO_2 film does not contain carbon black additive. The current density is defined to the illuminated area.

thermodynamically allowed. However, this effect is observed when the light power is ≥ 50 mW cm^{-2} suggesting that only a small proportion of photoelectrons at CB of Cu_2O can kinetically induce the lithiation process. In our energetic model, TiO_2 film has two interfaces: Cu_2O/TiO_2 and TiO_2/electrolyte. In the first interface, the two semiconductors equilibrate matching their Fermi levels, while the second is determined by the TiO_2/Li_xTiO_2 redox process. Therefore, the photoelectrons from the CB in Cu_2O would be mainly transferred into the CB of TiO_2 and only the electrons with enough energy above the work function of TiO_2/Li_xTiO_2 could induce the intercalation of Li^+ ions. Instead, the anodic sweep behavior suggests that the photoholes generated in the VB of Cu_2O are efficiently injected to the Li_xTiO_2 specie promoting the delithiation process since the photoholes cannot be injected to the VB of TiO_2.

Further information can be obtained chopping light during a cathodic linear sweep voltammetry (LSV) at 0.2 mV s^{-1} from ≈2.6 V (open circuit voltage, OCV) to 1.6 V versus Li/Li^+, Figure 3c. Large negative (positive) transient spike photocurrents are generated before the photocurrent stabilizes when the light is switched on (off). The presence of these transient current spikes indicates the discrepancy between the fast carrier generation and recombination and slow dynamics of the induced electrochemical process.[41] These transient spikes are significantly reduced when the conductive carbon additive is removed from the TiO_2 film, Figure 3d, suggesting that carbon black can accept very fast the photocharges but it does not contribute to the electrochemical process. More importantly, the current difference between dark and light condition increases significantly when the carbon additive is removed. In dark, the OCV corresponds to the difference between the Fermi level of Cu_2O and Li/Li^+. As the voltage decreases up to 1.6 V versus Li/Li^+ and the Fermi level of Cu_2O lifts up matching with the empty Li_xTiO_2 states, a dark current appears in the LSV plot. Under light irradiation, the observed photocurrent indicates that photoelectrons from the CB of Cu_2O are injected to the empty Li_xTiO_2 states and the lithiation process develops. This effect is especially relevant at 2 V versus Li/Li^+ and below indicating that at this voltage the photoelectrons induce lithiation process. The negligible photocurrent observed for plain ITO or ITO/Cu_2O (Figure S10, Supporting Information) confirms that photocharges generated in the Cu_2O are transferred to TiO_2 film to assist the adsorption/intercalation of Li^+ ions. Besides, both XPS (Figure S11, Supporting Information) and XRD (Figure S12, Supporting Information) spectra were registered for the photoelectrode after the LSV at 1.6 V. The results show the incorporation of Li in the electrode while the state of oxidation of copper remains mainly in +1.

2.4. Performance of the Photorechargeable Battery Device

The Cu_2O-TiO_2 photoelectrode performance is studied in a prototype with lithium metal as anode. **Figure 4**a plots the first

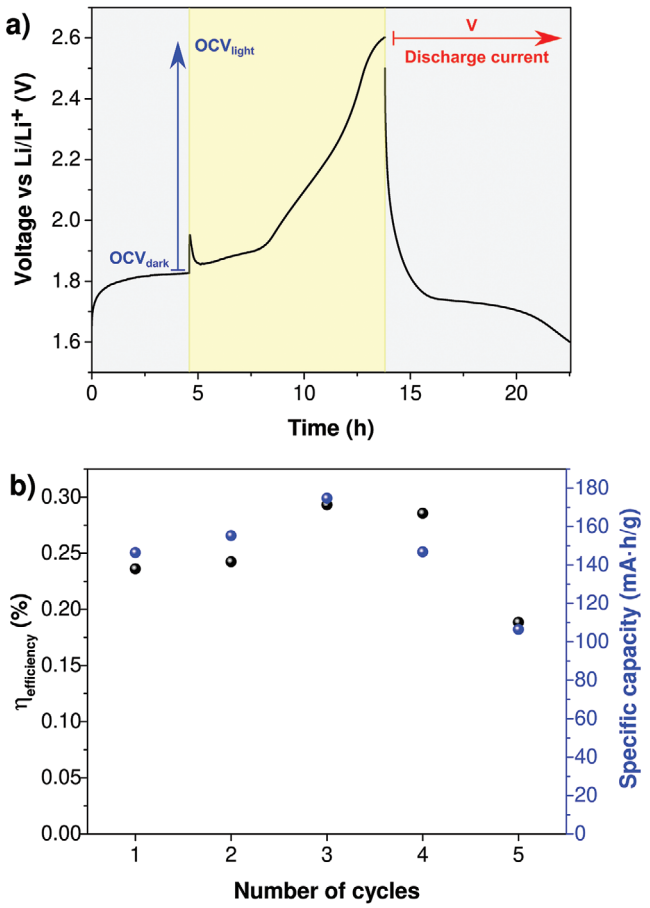

Figure 4. Cu_2O-TiO_2 as photocathode in lithium semibattery. a) Photocharge under light illumination and discharge in dark of the Cu_2O-TiO_2 photoelectrode of the first cycle. b) Discharge energy density and light to electrical energy efficiency calculated with Equation 1 of the photobattery after photocharging in open circuit until 2.6 V versus Li/Li^+ and discharging at 0.1C until 1.6 V versus Li/Li^+. TiO_2 film is prepared without carbon black additive.

light photocharge and discharge in dark. In dark, after a previous initial discharging step, the OCV slightly increases until it stabilizes at ≈1.8 V that is a lower voltage than the one in which delithiation reaction occurs. Then, the OCV increases when the LED light is turned on until it reaches 2.6 V after 9 h. At that point, the LED is turned off and a discharge current equivalent to 0.1C is applied to the photobattery until the voltage limit of 1.6 V versus Li/Li^+. The battery provides 146 $mAhg^{-1}$, which is 87% of the theoretical energy density of TiO_2 capacitive material. This process is repeated 5 times obtaining similar energy density in dark after photocharging in open circuit, Figure 4b. The efficiency of the photobattery is calculated as the output electrical energy divided by the input light energy:

$$\eta_{\text{efficiency}} = \frac{\int V I_{\text{discharge}} dt_{\text{discharge}}}{P_{\text{light}} A t_{\text{irradiation}}} \times 100 \quad (1)$$

where V is the measured voltage during the discharge process at $I_{\text{discharge}}$ and $t_{\text{discharge}}$ the time to the voltage changes from 2.6 to 1.6 V. In the denominator, P_{light} is 100 mW cm^{-2}, A the illuminated area, and the time of irradiation ($t_{\text{irradiation}}$).

The photorechargeable battery efficiency increases from 0.24% to 0.29% in the three first cycles. The calculated efficiency is in the order of the reported values (0.03%-0.6%) for photorechargeable batteries based on lithium ion (Table S1, Supporting Information). The table differentiates mainly three systems: based on dye-sensitized solar cells, on special cathode ($Li-O_2$ and Li−S) in which the cathodic reaction is photoassisted, and the host-based cathode and lithium anode like our system although in our case the light harvester is a different material than the host material. After three cycles, both the energy density and the efficiency of the photobattery start to decrease, presumably due to electrolyte degradation and/or accumulation of Li^+ ions that are not reduced in the lithium anode during charging process. However, we anticipate that since Cu_2O semiconductor can inject both electrons and holes to the Li_xTiO_2 material depending on the voltage, a completely regenerative photorechargeable battery can be fabricated with a suitable cathode. According to our bibliographic revision to date (Table S1, Supporting Information), lithium foil is usually employed as the anode of photorechargeable-based lithium batteries. Those devices and our system can be considered as lithium photorechargeable batteries of first generation type because the lithium will be depleted in long term due to the lack of enough voltage bias to back the anode to its reduced oxidation state Li(0).

3. Conclusion

This study describes the design of a photoelectrode composed of p-Cu_2O semiconductor as light harvester and n-type TiO_2 as capacitive element. The CV of the photoelectrode at different light powers shows that Cu_2O light harvester can inject photoelectrons and photoholes to Li_xTiO_2 empty or filled states to induce the lithiation and delithiation processes. The photoholes generated in the Cu_2O film can efficiently boost the deintercalation process from Li_xTiO_2 specie. However, the photoelectrons from the CB are less efficient and its effect is only observed after reaching a determined light power. We propose the existence of a kinetic limitation during lithium charge transfer and lithium diffusion explaining that only a small portion of the photoelectrons in the CB of Cu_2O can induce the lithiation process.

Finally, a photorechargeable battery device is fabricated and its performance is tested. The photorechargeable battery can be charged in ≈9 h only with light energy in an open circuit obtaining the ≈87% of the cathode energy density and with an efficiency up to 0.29%. However, after three cycles the efficiency and energy density decreases probably because the electrolyte starts to degrade and/or the accumulation of Li^+ ions in the electrolyte hinders further delithiation process of the photocathode.

This study provides rules to advance in the development of photorechargeable batteries. Among the different research directions, we highlight: i) the change of lithium metal for another electrode to build a device fully reversible, ii) the change of liquid organic electrolyte for solid electrolyte, and iii) the design of capacitive materials without limiting kinetic constraints.

4. Experimental Section

Deposition of Cu_2O Film and TiO_2 Nanoparticles: Cu_2O electrodeposition is an adapted process from the literature.[27,42] In short, NaOH pellets (Labkem) basify the solution of 0.45 M $CuSO_4$ (Probus) and 3 M Lactic Acid (Fluka) to pH 13. Cu_2O film deposits on ITO/PET substrate (30 Ω sq^{-1}, XOP Glass) in an electrodeposition process of two-electrodes with a cathodic current of 200 μAcm^{-2} during 150 min with Pt wire as a reference and counter electrode. The Cu_2O films were then rinsed with distilled water and dried in air.

A controlled hydrolysis of titanium isopropoxide (≥97.0%, Aldrich) provides TiO_2 nanoparticles as follows [43]: i) 600 μL of distilled water was added to a volumetric flask containing 20 mL of 2-propanol (>98.0%, FischerSci) and 600 μL of titanium isoproxide with continuous stirring, ii) the suspension was heated at a boiling point during 6 h keeping the stirring and using a reflux system to avoid the change in the solvent volume, and iii) the suspension was filtered, dried at 120 °C during 2 h and heat treated at 400 °C during 4 h to obtain the anatase phase in the TiO_2. The heating temperatures and times were determined after a DSC and TGA analysis (Figure S1, Supporting Information).

A Ru2500 diffractometer from RIGAKU performed XRD measurements on Cu_2O film using Cu Kα radiation between 20 and 80° 2θ at a scan rate of 0.03° s^{-1} and 0.03° scan step. TiO_2 powder XRD measurements were performed on a PANalytical Empyrean diffractometer between 15 and 80° 2θ using a scan step of 0.0131°. A FEG INSPECT-50 (FEI Company) took the SEM images. A UV–vis–NIR Jasco V6700 equipped with an ISN-723 integrating sphere and PbS photoconductive cell detector measured total reflectance in the 200–1400 nm range of TiO_2 powders diluted in $BaSO_4$ and both the reflectance and the transmittance of Cu_2O films in the 200–1300 nm range. The pseudo absorption $F(R_\infty)$ of Cu_2O film was calculated using both the reflectance and the transmittance data (Figure S2a–c, Supporting Information). The Kubelka–Munk transformation of the reflectance data of TiO_2 determined its pseudo absorbance. The extrapolation to zero y-axis of the Tauc plot (indirect and direct allowed bandgap setting for TiO_2 and Cu_2O respectively) [44] allows an optical bandgap estimation of the samples.; A XPS X-Ray Photoelectron Spectroscopy AXIS SupraTM from Kratos with monochromated Al Kα = 1486.6 eV and UPS He – Iα = 21.2 eV radiation source analyzed electronic transitions on the surface of the samples. A copper tape held the powder samples before a stream of compressed air removed the excess material. The vacuum chamber hosted the sample at pressure below 7×10^{-9} Torr. Adventitious carbon (284.8 eV) was the reference peak in XPS data treatment. The software CasaXPS fitted the peak traces. The Fermi edge (E_F = 0 eV) and Au $4f_{7/2}$ (84.0 eV) on a clean Au surface calibrated the binding energy for UPS measurements (Figure S3, Supporting Information).The doctor-blade deposition technique extended a slurry consisting of TiO_2:PVDF (AlfaAesar):carbon black Super P (99+, AlfaAesar) 85:5:10 weight ratio in N-Methyl Pyrrolidone (Sigma–Aldrich). Eventually, TiO_2:PVDF without carbon black replaced this layer as indicated in the text. TiO_2 deposits on Cu foil for electrochemical characterization and on the top of Cu_2O film previously electrodeposited on ITO substrate for photoelectrochemical study. Lithium foil (thickness 0.38 mm, Sigma–Aldrich) worked as a reference and counter electrode, which means the electrochemical study was performed on semibattery configuration. The battery cells were coin cells CR2032 crimped with hydraulic press (TMAXCN) inside an Ar glovebox (VAC-ATM). The electrolyte was 1 M $LiPF_6$ in EC:DEC (1:1) (v:v) solution (Sigma–Aldrich) embedded in fiber glass separator (Grade GF/C, Whatman glass). For photoelectrochemical characterization CR2032 coin cells were modified with a window (circular holes of 0.8 and 0.5 cm diameter in the positive case) allowing direct light irradiation of the photoelectrode, Figure S4a (Supporting Information). Besides, an indium ring replaced the metallic spring between the holed spacer and the case. This indium ring melted during the crimping process assuring a good electric contact and a good sealing of the cell, Figure S4b (Supporting Information). The electrochemical measurements were performed with a potentiostat–galvanostat Autolab M204 equipped with two channels and an optical bench equipped with white light LED (Figure S5, Supporting Information). LED power was set at one Sun (100 mW cm^{-2}) unless otherwise stated. LED power was measured with a Si-based photodetector (Figure S6), previously calibrated with a PVE300 system (Bentham) equipped with Si and Ge photodetectors.

Supporting Information

Supporting Information is available from the Wiley Online Library or from the author.

Acknowledgements

M.H. acknowledges the funding support from MCIN/AEI/10.13039/501100011033 and European Union "ESF Investing in your future" for the Ramón y Cajal fellowship (RYC2018-025222-I) and the project PID2019-108247RA-I00. E.J.J.-P. acknowledges the funding support from MCIN/AEI/ 10.13039/501100011033 and European Union NextGenerationEU/ PRTR (project grants PID2019-107893RB-I00 and EIN2020-112315, respectively). The authors also acknowledge the Diputación General de Aragón under the projects LMP71_21, E31_20R (M.H. and I.C.-R.) and T57_20R (E.J.J.-P.). The authors would like to acknowledge the use of Servicio General de Apoyo a la Investigacion-SAI, Universidad de Zaragoza.

Conflict of Interest

The authors declare no conflict of interest.

Data Availability Statement

The data that support the findings of this study are available from the corresponding author upon reasonable request.

Keywords

Cu_2O, lithium-ion batteries, photocathodes, photoelectrodes, photorechargeable batteries

Received: February 15, 2023
Published online:

[1] G. Hodes, J. Manassen, D. Cahen, *Nature* **1976**, *261*, 403.
[2] A. Fujishima, K. Honda, *Nature* **1972**, *238*, 37.
[3] S. N. Frank, A. J. Bard, *J. Phys. Chem.* **1977**, *81*, 1484.
[4] A. Hauch, A. Georg, U. O. Krašovec, B. Orel, *J. Electrochem. Soc.* **2002**, *149*, A1208.
[5] H. Nagai, H. Segawa, *Chem. Commun.* **2004**, *9*, 74.
[6] Y. Saito, A. Ogawa, S. Uchida, T. Kubo, H. Segawa, *Chem. Lett.* **2010**, *39*, 488.
[7] Y. Saito, S. Uchida, T. Kubo, H. Segawa, *Thin Solid Films* **2010**, *518*, 3033.
[8] P. Liu, H. Yang, X. Ai, G. Li, X. Gao, *Electrochem. Commun.* **2012**, *16*, 69.
[9] N. Yan, G. Li, G. Pan, X. Gao, *J. Electrochem. Soc.* **2012**, *159*, A1770.
[10] M. Yu, X. Ren, L. Ma, Y. Wu, *Nat. Commun.* **2014**, *5*, 5111.
[11] Y. Liu, N. Li, S. Wu, K. Liao, K. Zhu, J. Yi, H. Zhou, *Energy Environ. Sci.* **2015**, *8*, 2664.

[12] Y. Liu, N. Li, K. Liao, Q. Li, M. Ishida, H. Zhou, *J. Mater. Chem. A* **2016**, *4*, 12411.
[13] N. Li, Y. Wang, D. Tang, H. Zhou, *Angew. Chem., Int. Ed.* **2015**, *54*, 9271.
[14] A. Paolella, C. Faure, G. Bertoni, S. Marras, A. Guerfi, A. Darwiche, P. Hovington, B. Commarieu, Z. Wang, M. Prato, *Nat. Commun.* **2017**, *8*, 14643.
[15] Z. Wang, H. C. Chiu, A. Paolella, K. Zaghib, G. P. Demopoulos, *ChemSusChem* **2019**, *12*, 2220.
[16] Y.-Y. Gui, F.-X. Ai, J.-F. Qian, Y.-L. Cao, G.-R. Li, X.-P. Gao, H.-X. Yang, *J. Mater. Chem. A* **2018**, *6*, 10627.
[17] C. Andriamiadamanana, I. Sagaidak, G. Bouteau, C. Davoisne, C. Laberty-Robert, F. Sauvage, *Adv. Sustainable Syst.* **2018**, *2*, 1700166.
[18] S. Ahmad, C. George, D. J. Beesley, J. J. Baumberg, M. De Volder, *Nano Lett.* **2018**, *18*, 1856.
[19] A. Lee, M. Vörös, W. M. Dose, J. Niklas, O. Poluektov, R. D. Schaller, H. Iddir, V. A. Maroni, E. Lee, B. Ingram, *Nat. Commun.* **2019**, *10*, 4946.
[20] A. Kumar, P. Thakur, R. Sharma, A. B. Puthirath, P. M. Ajayan, T. N. Narayanan, *Small* **2021**, *17*, 2105029.
[21] B. D. Boruah, A. Mathieson, B. Wen, S. Feldmann, W. M. Dose, M. De Volder, *Energy Environ. Sci.* **2020**, *13*, 2414.
[22] B. D. Boruah, B. Wen, S. Nagane, X. Zhang, S. D. Stranks, A. Boies, M. De Volder, *ACS Energy Lett.* **2020**, *5*, 3132.
[23] B. Deka Boruah, A. Mathieson, S. K. Park, X. Zhang, B. Wen, L. Tan, A. Boies, M. De Volder, *Adv. Energy Mater.* **2021**, *11*, 2100115.
[24] B. D. Boruah, B. Wen, M. De Volder, *Nano Lett.* **2021**, *21*, 3527.
[25] S. Safshekan, I. Herraiz-Cardona, D. Cardenas-Morcoso, R. Ojani, M. Haro, S. Gimenez, *ACS Energy Lett.* **2017**, *2*, 469.
[26] A. Lemsi, D. Cardenas-Morcoso, M. Haro, C. Gil-Barrachina, C. Aranda, H. Maghraoui-Meherzi, M. García-Tecedor, S. Giménez, B. Julián-López, *Energy Technol.* **2020**, *8*, 2000301.
[27] A. Paracchino, V. Laporte, K. Sivula, M. Grätzel, E. Thimsen, *Nat. Mater.* **2011**, *10*, 456.
[28] L. Liu, W. Yang, W. Sun, Q. Li, J. K. Shang, *ACS Appl. Mater. Interfaces* **2015**, *7*, 1465.
[29] M. E. Aguirre, R. Zhou, A. J. Eugene, M. I. Guzman, M. A. Grela, *Appl. Catal., B* **2017**, *217*, 485.
[30] D. Tahir, S. Tougaard, *J. Phys.: Condens. Matter* **2012**, *24*, 175002.
[31] G. Shao, *Energy Environ. Mater.* **2021**, *4*, 273.
[32] J.-N. Nian, C.-C. Tsai, P.-C. Lin, H. Teng, *J. Electrochem. Soc.* **2009**, *156*, H567.
[33] Y. Yang, D. Xu, Q. Wu, P. Diao, *Sci. Rep.* **2016**, *6*, 35158.
[34] F. Caballero-Briones, J. M. Artés, I. Díez-Pérez, P. Gorostiza, F. Sanz, *J. Phys. Chem. C* **2009**, *113*, 1028.
[35] V. Aravindan, Y.-S. Lee, R. Yazami, S. Madhavi, *Mater. Today* **2015**, *18*, 345.
[36] C. Maheu, L. Cardenas, E. Puzenat, P. Afanasiev, C. Geantet, *Phys. Chem. Chem. Phys.* **2018**, *20*, 25629.
[37] W. Zhang, D. Wang, W. Zheng, *J Energy Chem* **2020**, *41*, 100.
[38] A. Stashans, S. Lunell, R. Bergström, A. Hagfeldt, S.-E. Lindquist, *Phys. Rev. B* **1996**, *53*, 159.
[39] J. Wang, J. Polleux, J. Lim, B. Dunn, *J. Phys. Chem. C* **2007**, *111*, 14925.
[40] S. J. An, J. Li, C. Daniel, D. Mohanty, S. Nagpure, D. L. Wood III, *Carbon* **2016**, *105*, 52.
[41] Z. Lian, Y. Tao, Y. Liu, Y. Zhang, Q. Zhu, G. Li, H. Li, *ACS Appl. Mater. Interfaces* **2020**, *12*, 44731.
[42] S. Hussain, C. Cao, Z. Usman, Z. Chen, G. Nabi, W. S. Khan, Z. Ali, F. K. Butt, T. Mahmood, *Thin Solid Films* **2012**, *522*, 430.
[43] P. Acevedo-Peña, M. Haro, M. E. Rincón, J. Bisquert, G. Garcia-Belmonte, *J. Power Sources* **2014**, *268*, 397.
[44] C. Malerba, F. Biccari, C. L. A. Ricardo, M. D'Incau, P. Scardi, A. Mittiga, *Sol. Energy Mater. Sol. Cells* **2011**, *95*, 2848.